Layer-dependent band alignment of few layers of blue phosphorus and their van der Waals heterostructures with graphene

Renato B. Pontes,[1,*] Roberto H. Miwa,[2,†] Antônio J. R. da Silva,[3,4,‡] Adalberto Fazzio,[5,6,§] and José E. Padilha[7,‖]

[1]*Instituto de Física, Universidade Federal de Goiás, Campus Samambaia, 74690-900 Goiânia, GO, Brazil*
[2]*Instituto de Física, Universidade Federal de Uberlândia, Caixa Postale 593, 38400-902 Uberlândia, MG, Brazil*
[3]*Instituto de Física, Universidade de São Paulo, Caixa Postale 66318, 05315-970 São Paulo, SP, Brazil*
[4]*Laboratório Nacional de Luz Síncrotron, Caixa Postale 6192, 13083-970 Campinas, SP, Brazil*
[5]*Brazilian Nanotechnology National Laboratory (LNNano)/CNPEM, P.O. Box 6192, 13083-970 Campinas, SP, Brazil*
[6]*Centro de Ciências Naturais e Humanas, Universidade Federal do ABC, 49960-001, Brazil*
[7]*Campus Avançado Jandaia do Sul, Universidade Federal do Paraná, 86900-000 Jandaia do Sul, PR, Brazil*

(Received 10 April 2018; revised manuscript received 31 May 2018; published 12 June 2018)

The structural and electronic properties of few layers of blue phosphorus and their van der Waals heterostructures with graphene were investigated by means of first-principles electronic structure calculations. We study the four energetically most stable stacking configurations for multilayers of blue phosphorus. For all of them, the indirect band-gap semiconductor character, are preserved. We show that the properties of monolayer graphene and single-layer (bilayer) blue phosphorus are preserved in the van der Waals heterostructures. Further, our results reveal that under a perpendicular applied electric field, the position of the band structure of blue phosphorus with respect to that of graphene is tunable, enabling the effective control of the Schottky barrier height. Indeed, for the bilayer blue phosphorene on top of graphene, it is possible to even move the system into an Ohmic contact and induce a doping level of the blue phosphorene. All of these features are fundamental for the design of new nanodevices based on van der Waals heterostructures.

DOI: 10.1103/PhysRevB.97.235419

I. INTRODUCTION

The unavoidable end of the road for the silicon technology has boosted the recent development of nanoelectronics using two-dimensional (2D) [1,2] materials. The whole area of 2D materials [3–6] was driven by the isolation of a monolayer graphene [7]. Those materials have been showing unusual physical properties and have been demonstrating huge potential for improving nanodevices beyond Moore's law [8].

A lot of attention has been devoted to monoelemental two-dimensional materials. Those 2D materials can be found in groups III, IV, and V of the periodic table [9]. Looking into group III, we have the elemental 2D boron material, named borophene [10,11]. This material possesses several crystal structures, all of them exhibiting metallic character. A chemically modified borophene, such as hydrogenated 2D borophene, is predicted to be dynamically stable and present massless Dirac fermions as graphene [12,13]. In group IV, graphene, a material that exhibits remarkable properties, is an allotrope of elemental carbon. The other elemental 2D materials in this group are based on silicon, germanium, and tin atoms. Silicene, germanene, and stanene have buckled honeycomb structures with a mixed sp^2-sp^3 hybridization. Those structures that have been theoretically predicted to exist and have already been experimentally synthesized [14–16] present topologically nontrivial electronic states, being considered 2D quantum spin Hall insulators [17]. Moving to group V, phosphorene, arsenene, antimonene, and bismuthene have been successfully synthesized [18–21]. However, the most investigated and the main examples of van der Waals (vdW) layered materials, in this group, are those composed solely by phosphorus atoms [22–24].

Phosphorus exists in several polytypes; the most common are the reactive white and red phosphorus, and the relatively inert black phosphorus (BP) [18,22,23,25]. The bulk BP is the most stable phosphorus allotrope at room temperature and its monolayers are bounded by van der Waals interactions. BP has a puckered structure and, as a consequence, it exhibits physical and chemical properties which are strongly dependent on the direction considered. For example, the armchair direction presents a high mobility of around 10 000 $cm^2\,V^{-1}\,s^{-1}$, while the zigzag direction has a much lower mobility of 600 $cm^2\,V^{-1}\,s^{-1}$. The BP can be exfoliated and its monolayer is called phosphorene. It is a direct band-gap semiconductor, with a band gap of around 2 eV. These properties make phosphorene a potential candidate to be used in technological applications [26,27] ranging from nanotransistors to active elements in solar cells [28,29].

Recently, the family of the phosphorus-based materials has gained a new member, the blue phosphorus (blue-P). This material that was, firstly, predicted by *ab initio* calculations [30], has been synthesized on an Au(111) substrate by means of the molecular beam epitaxy technique [31,32]. The single-

*pontes@ufg.br
†hiroki@ufu.br
‡jose.roque@lnls.br
§fazzio@if.usp.br
‖jose.padilha@ufpr.br

layer blue-P consists of two atomic layers of P atoms in a buckled graphenelike structure. It exhibits an indirect band gap of roughly 2.0 eV and electronic mobility around 4.6×10^2 (4.7×10^1) $cm^2\,V^{-1}\,s^{-1}$ for the armchair (zigzag) direction, at room temperature [33].

In parallel with the efforts on the study of single-component layered materials, the research on vdW heterostructures, which are made by stacking layer by layer of different 2D crystals, has been gaining strength [34,35]. Such heterostructures have recently been fabricated and studied revealing exquisite properties and novel physical phenomena motivating intense scientific investigations [36–41]. In particular, phosphorus-based vdW heterostructures are quite promising for applications in nanoscale [42].

Since the experimental obtention of 2D blue phosphorus a number of studies have been conducted to understand the mechanical and electronic properties of monolayer and bilayer blue-P [30,43] and their vdW heterostructures with other 2D semiconductors [44,45]. However, a deep understanding of important physical properties such as the layer-dependent evolution of the band gap and band alignments, as well as the effects of the quantum confinement as a function of the number of layers in few layers of blue-P, are still lacking. Those properties are of paramount importance in the determination of the Schottky barrier. Hence, knowledge of the layer-dependent band alignment is fundamental for the design of new devices based on blue-P.

In this work, we systematically study the layer-dependent band alignment of few layers of blue phosphorus and their vdW heterostructures with graphene. Essentially, our main goals are (i) to investigate the evolution of the band-edge states as a function of the number of blue-P layers and the stacking configuration; (ii) to understand how the blue-P interacts with graphene; and (iii) to determine what are the contact barriers created in this interface and how they could be controlled.

II. COMPUTATIONAL DETAILS

In order to obtain the energetically most stable structures and the electronic properties of few layers of blue phosphorus and their vdW heterostructures with graphene, we performed first-principles total energy calculations within the density functional theory (DFT) framework as implemented in the VASP code [46,47]. The generalized gradient approximation, as proposed by Perdew-Burke-Ernzerhof (PBE-GGA) [48], is used for the exchange and correlation potential. The projector augmented wave potentials [49] are used to describe the interaction between valence electrons and ion cores. The plane-wave kinetic-energy cutoff is set at 400 eV. All atomic positions and lattice constants are optimized by using the van der Waals–density functional theory (vdW-DFT) optB88-vdW [50,51]. The positions of the atoms are allowed to relax until the force on each atom is smaller than 0.001 eV/Å. The electronic self-consistency criterion is set as 10^{-7} eV. For the multilayer unit cells, we used a k-point sampling of $7 \times 7 \times 1$ and for the supercell calculation the k-point sampling was $4 \times 4 \times 1$. To avoid the interaction between neighboring cells, we employed a vacuum region of 20 Å. Once the optimized structures are obtained, the screened hybrid functional of Heyd-Scuseria-Ernzerhof (HSE06) [52,53] is employed to calculate all the electronic properties of the blue phosphorus–based materials. Although we may have different parametrizations for the HSE functional, in order to improve the calculated values of energy-gap and band-edge position, we have used the standard HSE06 approach, which provides proper results for the blue-P system and other two-dimensional materials [54,55], when compared with the current literature.

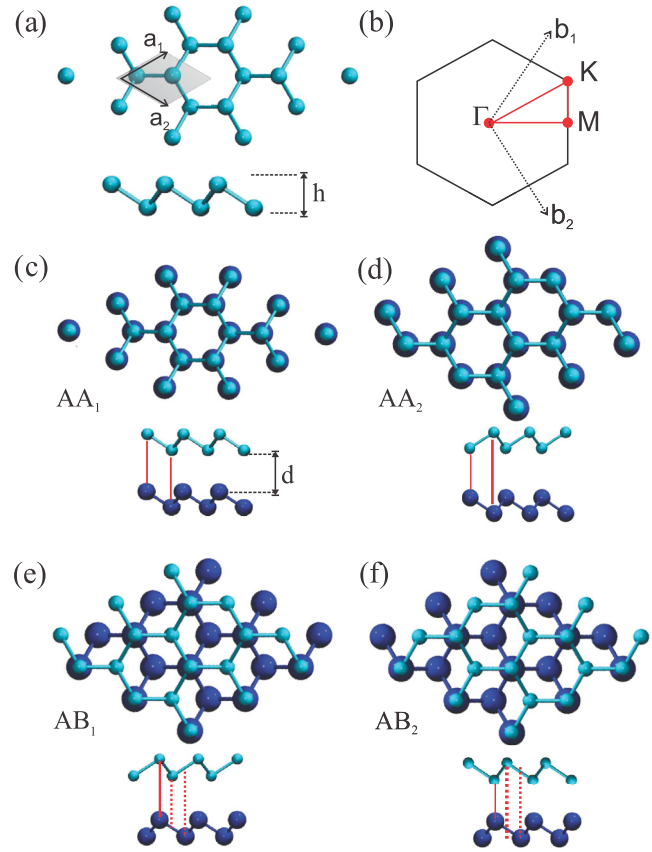

FIG. 1. (a) Top panel: A ball-and-stick representation of the structure of a single layer of blue phosphorus. The lattice vectors ($\mathbf{a_1}$ and $\mathbf{a_2}$) that define the unit cell (gray region) are also indicated. Bottom panel: A side view of the blue phosphorus monolayer. Dashed black lines indicate the buckling height, h. (b) Schematic representation of the first Brillouin zone of a hexagonal lattice. The reciprocal lattice vectors ($\mathbf{b_1}$ and $\mathbf{b_2}$) and the high-symmetry points are highlighted. (c)–(f) Top and side views of the four stacking configurations considered in our calculations. The different colors in the P atoms are used to distinguish the upper from lower layers. The distance, d, between the layers is also shown. The solid (dashed) red lines in (c)–(f) represent the atoms that are located on the top of other P atoms (center of an hexagon).

III. RESULTS AND DISCUSSIONS

In Fig. 1(a) is depicted a single layer of blue phosphorus. The crystal structure consists of phosphorus atoms arranged in a honeycomb lattice defined by the $\mathbf{a}_{1,2}$ unit-cell vectors, such as graphene, with an additional feature that it has a buckled conformation. The two sublattice planes are separated by a distance $h \approx 1.2$ Å, as shown in the bottom panel of Fig. 1(a). For the monolayer, we obtained a lattice constant of

TABLE I. Total energy difference (in meV/atom) between the energetically most stable structure (named AA_1) and the other considered stacks on the DFT-vdW calculations. The lattice parameter, a, and the interlayer distance, d, are presented as well.

Stacking	ΔE_{total} (meV/atom)	a (Å)	d (Å)
AA_1	0	3.31	3.40
AB_1	2	3.31	3.37
AB_2	36	3.30	3.97
AA_2	48	3.30	3.98

$a = 3.29$ Å, in agreement with the values previously reported in the literature [30–32]. The crystal lattice of blue-P is different from black phosphorus, which has a puckered orthorhombic layered structure [23]. However, through a combination of transformations, black phosphorus could be converted to blue phosphorus [30].

Few layers of blue-P can be constructed by stacking two or more monolayers. In contrast to graphene, which has only two stacking sequences, the monolayer blue-P presents a low-buckled structure. Thus, additional stacking configurations between the layers are possible. In Figs. 1(c)–1(f), we show the four possible stacking modes, named AA_1, AA_2, AB_1, and AB_2. These additional modes are due to the A and B sites of the hexagonal lattice, in the same layer, being located at different planes. For example, the top/bottom layer could be stacked with the same buckling order [AA_1; Fig. 1(c)], or reversed [AA_2; Fig. 1(d)]. In the AB_1 and AB_2 [Figs. 1(e) and 1(f)], or Bernal-stacked form, half of the atoms lie directly over the center of a hexagon in the lower blue-P sheet [indicated by the red dashed lines in Figs. 1(e) and 1(f), side view], and half of the atoms lie over a phosphorus atom [indicated by the red solid line in Figs. 1(e) and 1(f), side view]. The colors of the atoms in Fig. 1 are used only to differentiate the layers of the system.

The calculated energetically most stable stacking order of bilayer blue phosphorus layers is AA_1 followed by AB_1, AB_2, and AA_2, having 2, 36, and 48 meV/atom higher energies than AA_1. The total energy differences between the four investigated stacks are quite small (meV order), typical of vdW layered materials [56–58]. Moreover, the results for the energetics of the stacking sequence are in good agreement with previous results obtained by Gosh *et al.* [43]. The energetics and structural parameters of the four bilayers conformations are summarized in Table I. For the AA_1 stacking mode, at the equilibrium distance (3.40 Å), the vdW-DFT calculated binding energy is about 104 meV/atom. Another remarkable point that we conclude from the results shown in Table I, is that the lattice constant remains unaltered, independently of the stacking configuration, while the interlayer distance, d, strongly depends on the stacking order since it is intrinsically related to the interaction between p_z orbitals.

In Fig. 2 we show, for the (a) AA_1, (b) AA_2, (c) AB_1, and (d) AB_2 stacking modes, the calculated electronic band structures of blue phosphorus for $n = 1$–4 layers. The high-symmetry points are schematically shown in Fig. 1(b). The HSE06-DFT calculated band structure indicates that monolayer blue phosphorus is a semiconductor with an indirect band

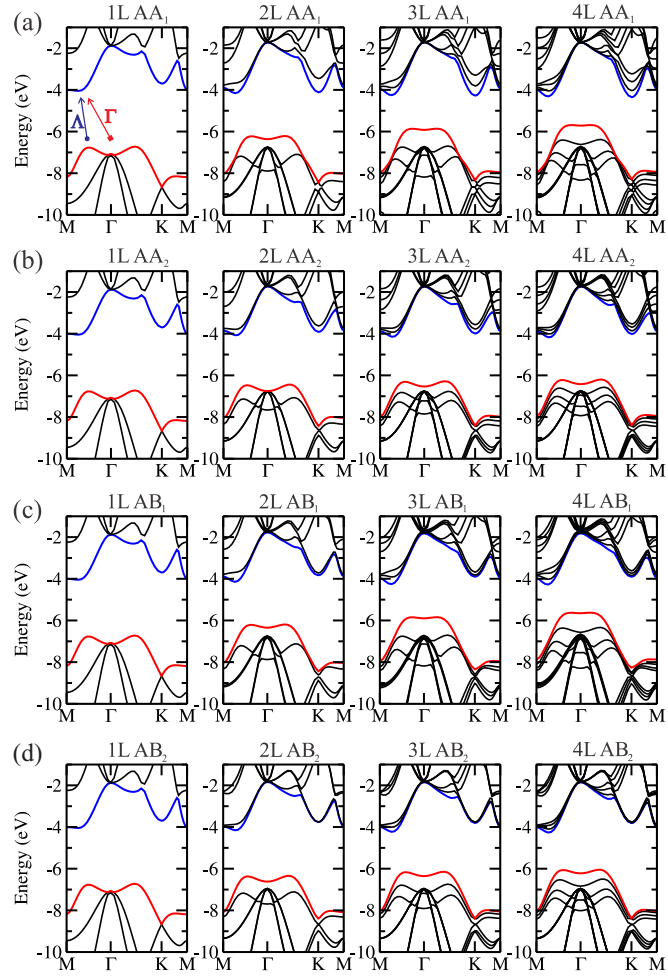

FIG. 2. Electronic band structures for one, two, three, and four layers of blue phosphorus in the stacking modes: (a) AA_1, (b) AA_2, (c) AB_1, and (d) AB_2. The valence and conduction bands are highlighted. All band structures were aligned with respect to the vacuum level. The arrows in (a) indicate the important band gaps (Λ and Γ). The single-layer band structure is repeated in (a), (b), (c), and (d) just for comparison.

gap ($E_{\text{gap}} \approx 2.7$ eV), in very good agreement with previous reports in the literature [30,59]. Moreover, we verify that neither the valence-band (VB) maximum nor the conduction-band (CB) minimum is located at any high-symmetry point in the Brillouin zone but both are found approximately in the middle of M and Γ. Another point similar to VB can also be observed between Γ and K, thus the VB seems to be degenerated in two distinct points.

For the AA_1 stacking configuration [Fig. 2(a)], the CB is always located in a valley between M and Γ independently of the number of layers. Initially, the VB is located in a point between M and Γ. If the number of layers is increased, the valence band becomes nearly flat around the Γ point, and in this way for more than four layers, it becomes located at Γ. The same behavior occurs for the AB_1 configuration, shown in Fig. 2(c). For the AA_2 and AB_2 stacks, the conduction band behaves like in the other configurations, whereas the valence band is always located in a k point between M and Γ. The same behavior is observed for all stacking configurations, when

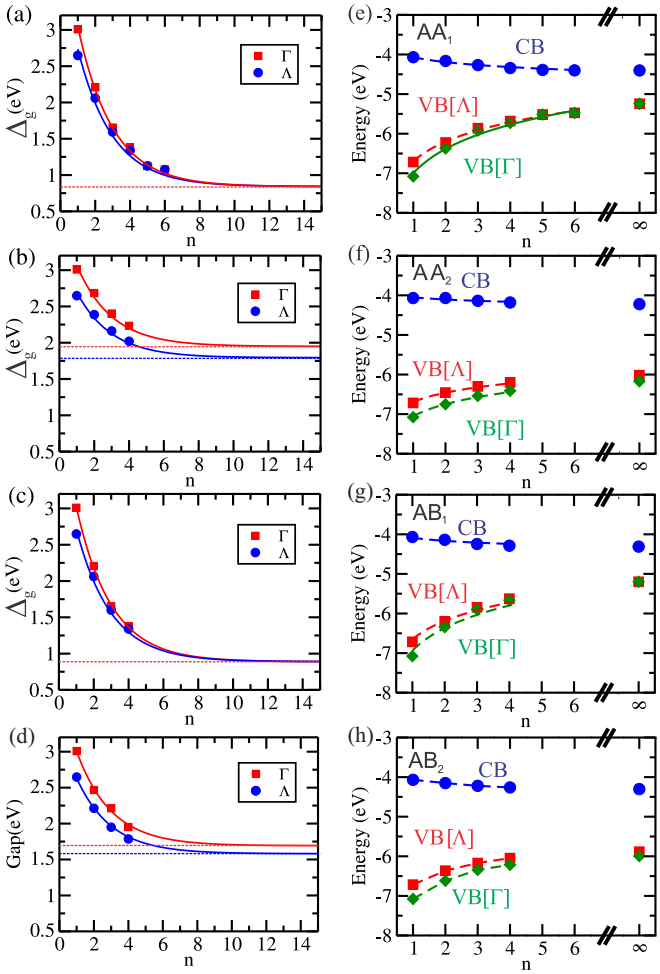

FIG. 3. Band gaps Δ_g^{Γ} and Δ_g^{Λ} as a function of the number of layers for (a) AA_1, (b) AA_2, (c) AB_1, and (d) AB_2. The HSE06-DFT calculated band gaps are indicated by the solid squares and circles. The fitting curves are presented by the solid lines. The horizontal dashed lines indicate the bulk ($n \to \infty$) band gaps. (e)–(h) Evolution of the band edges as a function of the number of layers for the stacks AA_1, AA_2, AB_1, and AB_2, respectively.

we go to the bulk of the materials, where the valence band is located at the Γ point for the AA_1 and AB_1 materials, whereas for the AA_2 and AB_2 it is located between M and Γ (see Fig. S1 in the Supplemental Material [60]). One important point to note is that the behavior of the band structure for all stacking configurations is strongly related to the interlayer distance and consequently, related to the interaction of the out-of-plane orbitals of each layer. For example, for the AA_1 and AB_1, the interlayer distance (see Table I) is smaller when compared to the AA_2 and AB_2, and the interaction between the layers is maximized in this case. In this way, the effect of the quantum confinement is stronger in the stackings AA_1 and AB_1, when compared to AA_2 and AB_2. This effect has direct consequences in the evolution of the band gap of the materials. However, we verify that for all investigated stacking configurations, the multilayers of blue-P preserve their indirect band-gap semiconducting character.

In Figs. 3(a)–3(d) we show the evolution of the band gap as a function of the number of layers n for the AA_1, AA_2, AB_1, and AB_2 configurations. The band gaps decrease monotonically and it could be tunable depending on the number of layers. For the AA_1 and AB_1 stacks, their dependence with the number of layers are almost the same, and they reach almost the same value at the bulk limit $n \to \infty$, where the bulk band gap for the AA_1 is 0.84 eV and for the AB_1 is 0.89 eV. However, if we look to the AA_2 and AB_2 stackings presented in Figs. 3(b) and 3(d), the band gap has a small variation with respect to the number of layers, converging rapidly to the bulk value (represented by the dashed lines in each figure). In this multilayer material, even though the layers are held by weak van der Waals interactions, the stacking order plays an important role in the quantum confinement effect of the band gap and band alignments, as we have previously observed in the band-structure calculations.

TABLE II. Adjust equations for the the band gaps Δ_g^{Γ} and Δ_g^{Λ}, at different stacking modes, as a function of the number of blue-P layers.

Stacking	Δ_g^{Γ} (eV)	Δ_g^{Λ} (eV)
AA_1	$0.84 + 3.63e^{-n/2}$	$0.84 + 3.12e^{-n/2}$
AA_2	$1.95 + 1.84e^{-n/2}$	$1.79 + 1.48e^{-n/2}$
AB_1	$0.89 + 3.51e^{-n/2}$	$0.89 + 3.01e^{-n/2}$
AB_2	$1.69 + 2.16e^{-n/2}$	$1.58 + 1.73e^{-n/2}$

One important point is to determine the relationship between the band gap $E_g(n)$ and the number of layers, n, of the few-layer 2D material. To this end, we have fitted the band gap of an arbitrary multilayer blue-P, using a single parameter exponential expression

$$\Delta_g(\text{eV}) = E_g(\text{bulk}) + Ae^{-n/2},$$

where E_g(bulk) is the electronic band gap of bulk blue-P and A is a fitting parameter. The adjust equations for the band gaps Δ_g^{Γ} and Δ_g^{Λ}, at different stacking modes, are summarized in Table II. According to those equations, the band gaps as a function of the number of layers are plotted in Figs. 3(a)–3(d) (solid lines). This behavior is related to the reduction of the quantum confinement as a function of increasing the thickness of the material.

It is worth mentioning that other fittings can also be made in order to capture the effects of quantum confinement as a function of the number of layers. Most of them are based on a power law of the band gap as a function of the number of layers [54,61–63]. However, in those fittings are used two adjustment parameters and, even so, they do not correctly capture the energy gap value of the monolayer, which is possibly related to the absence of interlayer coupling in the monolayer limit. However, using an exponential function, as presented in this investigation, the monolayer limit is fitted very well. One reason is that the evolution of the band gap is not only governed by interlayer coupling effects, but also due to surface effects. The monolayer limit, the extreme case of the quantum confinement effect, is governed by surface energy effects, rather than the interlayer coupling. In this way, our exponential model captures the surface energy and interlayer coupling effects. A similar model was proposed by Zhang *et al.* for the multilayers of C_2N-$h2D$ [62]. For purposes of comparison, we

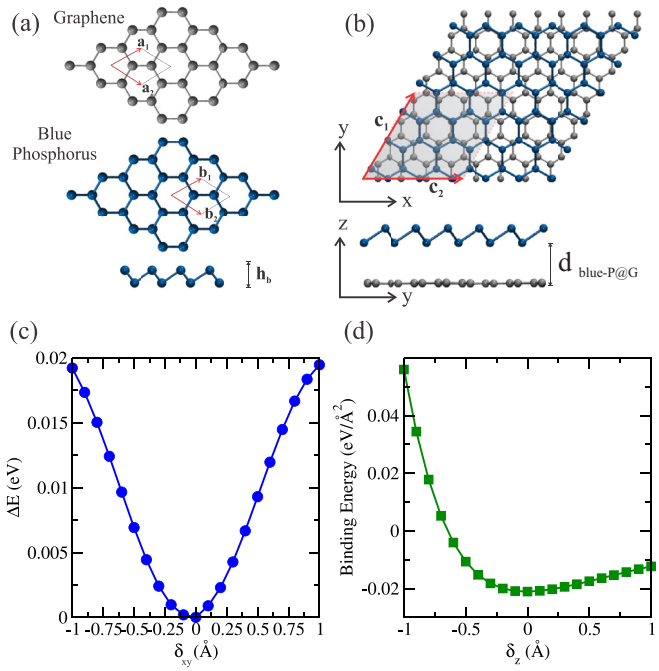

FIG. 4. (a) Schematic representations of single-layer graphene and blue phosphorus. The lattice vectors, $\mathbf{a_1}$ ($\vec{b}_1$) and $\mathbf{a_2}$ ($\vec{b}_2$), for graphene (blue phosphorus) are indicated. The buckling height, h_b, is also shown. (b) Top and side views of a monolayer blue phosphorus on top of graphene. The lattice vectors $\mathbf{c_1}$ and $\mathbf{a_2}$ that define the unit cell (light gray region) and the distance between monolayer graphene and blue phosphorus ($d_{\text{blue-P@G}}$) are shown. (c) Variation of the total energy (ΔE), in eV, as a function of displacements $\delta_{x,y}$ of the monolayer blue phosphorus relative to graphene. The zero was set as the total energy of the lowest energy configuration. (d) Binding energy as a function of the distance, δ_z, between blue-P and graphene. The zero was set as the equilibrium ($d^{\text{eq}}_{\text{blue-P@G}}$) distance.

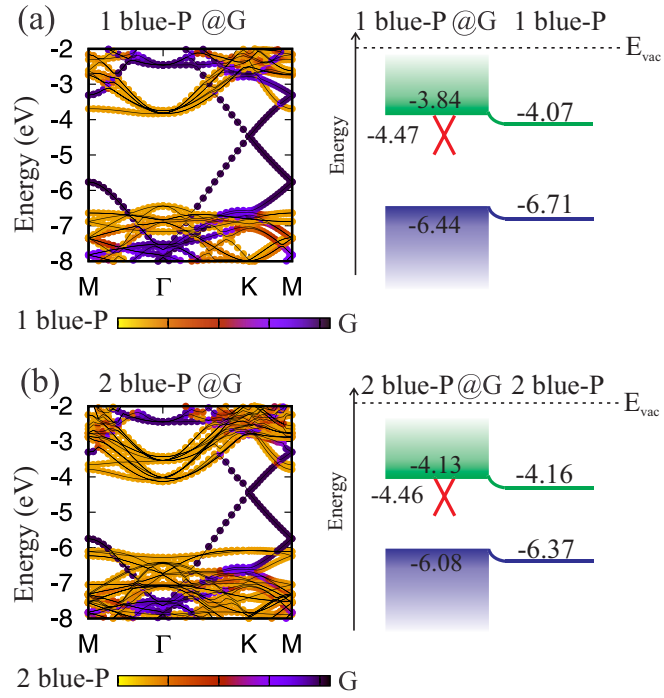

FIG. 5. Left panels: DFT-calculated project electronic band structures of single-layer blue-P (a) and bilayer blue-P (b) on graphene. Right panels: Schematic comparison between the band structures of the single-layer blue-P (bilayer blue-P) with graphene with pristine single-layer (bilayer) blue phosphorus in the vicinity of the Fermi level. The red crossed lines represent the Dirac cone of graphene. The scales indicate the magnitude of the projections. All band structures were aligned with respect to the vacuum level.

also conduct an adjustment based on a power law, which is presented in Fig. S2 in the Supplemental Material [60].

In Figs. 3(e)–3(h) we present the evolution of the band edges as a function of the number of layers for the different stacking orders. All band edges were aligned with an absolute energy scale, i.e., the vacuum level. This analysis is very important, because we can determine the band alignment between the different components of a vdW heterostructure, and this could also help in screening for 2D metals that will present ohmic contacts [34,35,64,65]. We verified that the top of the valence band VB[Λ,Γ] increases with the number of layers, whereas the conduction-band minimum CB remains almost constant. This occurs because, independently of the stacking sequence and number of layers, the states of the CB, which are mainly composed of s and $p_{x,y}$ orbitals, are weakly perturbed when more layers are added to the system. On the other hand, the valence bands, which are mainly composed of p_z orbitals, present a completely different behavior as a function of the number of layers and stacking sequence. When more than one layer is stacked together, the degeneracy is lifted, changing its position with respect to the vacuum level. Also, for the different stacking modes, the interactions between the p_z orbitals of the layers are also different, which also explains the different behaviors for the AA_1, AA_2, AB_1, and AB_2 systems.

If one wishes to use blue-P in electronic devices, to reach the best of its performance, one has to use as a metallic contact an element that preserves the electrical integrity of the system, without inducing effects, such as the Fermi-level pinning. In this paradigm, graphene has been considered a key element to be used as a metallic contact. Looking to the band-edge positions of blue-P, relative to the vacuum level, and comparing to the graphene Dirac position, which is close to −4.5 eV, we will see that the CB is closer to the graphene Dirac point. This indicates that the Schottky contact will be n type. This behavior is completely different from black phosphorus, which has a p-type Schottky contact [66].

To completely understand the behavior of blue-P in a possible device, contacted with graphene, we created a 2D van der Waals heterostructure of blue-P and graphene. It is worth noting that a similar study was made by Sun *et al.* [67], where they have studied a vdW heterostructure of a single-layer blue-P on top of a single-layer graphene and a single-layer gallium nitride. The prototypical systems considered in our work were composed by a single-layer and a bilayer blue phosphorus (at the lowest energy stacking configuration, the AA_1) on top of a single-layer graphene (1L blue-P@G and 2L blue-P@G). We initially examined the energetic stability of the composed heterostructure. In order to minimize the lattice mismatch between the graphene lattice constant [$a = 2.46$ Å; Fig. 4(a), top panel]

and the blue-P lattice constant [$b = 3.31$ Å; Fig. 4(a), bottom panel], we have considered surface periodicities of (3×3) and (4×4) for the blue-P and graphene, creating the supercell defined by the lattice vectors $\vec{c}_{1,2}$, as presented in Fig. 4(b). In this configuration, the graphene supercell is compressed by around 0.9% (0.3%/unit cell). The configuration depicted in Fig. 4(b) is the energetically most stable. It was obtained from several initial positions of the single-layer blue phosphorus in relation to the graphene. Once the lower energy configuration was obtained, we shifted laterally the monolayer blue-P with respect to graphene, by small amounts $\delta_{x,y}$, to ensure that the system was, in fact, the minimum energy configuration. In Fig. 4(c) we show the variation of the total energy difference as a function of $\delta_{x,y}$. As can be seen, the system is really on the minimum of energy. (The same behavior was observed for the 2L blue-P@G, not shown here.)

With the in-plane equilibrium configuration, we determined the binding energy of the blue-P layer in graphene per area unit, as presented in Fig. 4(d). The binding energy is given by $E_b = [E_{\text{blue-P@G}} - (E_{\text{blue-P}} + E_G)]/A$, where $E_{\text{blue-P@G}}$ is the total energy of the vdW heterostructure composed of blue-P and graphene at the most stable conformation, $E_{\text{blue-P}}$ is the total energy of the isolated blue-P and E_G is the total energy of the single-layer graphene, and A is the area of the supercell. For both the single and bilayer blue-P we obtained similar value for the binding energy, around 21 meV/Å^2, with an equilibrium distance of 3.47 Å. The blue-P and graphene binding energy are in the same order of magnitude as black phosphorus and graphene and that obtained by Sun *et al.* in [67] for a graphene/blue-P vdW heterostructure. The interlayer distances are also similar, as discussed in Ref. [66].

In Fig. 5, we show the projected electronic band structure for the single-layer (a) and bilayer blue phosphorus (b) on top of a monolayer graphene. As can be verified, the electronic structure of both blue-P and graphene are preserved upon the heterostructure formation, indicating that all properties of the isolated 2D materials are maintained, which is a signature of the vdW interaction. Also, the position of the Dirac point with respect to the vacuum level, in the composed heterostructure, remains almost constant, when compared to the freestanding graphene. Moreover, if we inspect the electronic band gap of blue-P on top of graphene with respect to the pristine one, we verify a decrease of the gap of 0.04 eV for the single-layer and 0.26 eV for the bilayer blue phosphorus.

In a device, if one wishes to use graphene as the metal contact and the single-layer or bilayer blue phosphorus as a channel, it is very important to know its Schottky barrier height (SBH). Using the Schottky-Mott rule, since there is no chemical bond between the materials, and there is no Fermi-level pinning effect, we obtained for the single layer a SBH of 0.63 eV, whereas for the bilayer it is 0.33 eV. In both vdW heterostructures, electrons will be the majority carriers, dominating the conduction. A similar behavior was observed in [67] for the single-layer blue-P on graphene, where they obtained an n-type Schottky barrier without any applied electric field. Additionally, even without any charge transfer between the single-layer and bilayer blue-P with graphene, if an in-plane device were made, there will be a band bending between the region of the blue-P on graphene and the freestanding one, as we can see from Figs. 5(a) and 5(b), right panel. As we can see, electrons will flow from the noncontacted blue phosphorene region to the contacted one, making the

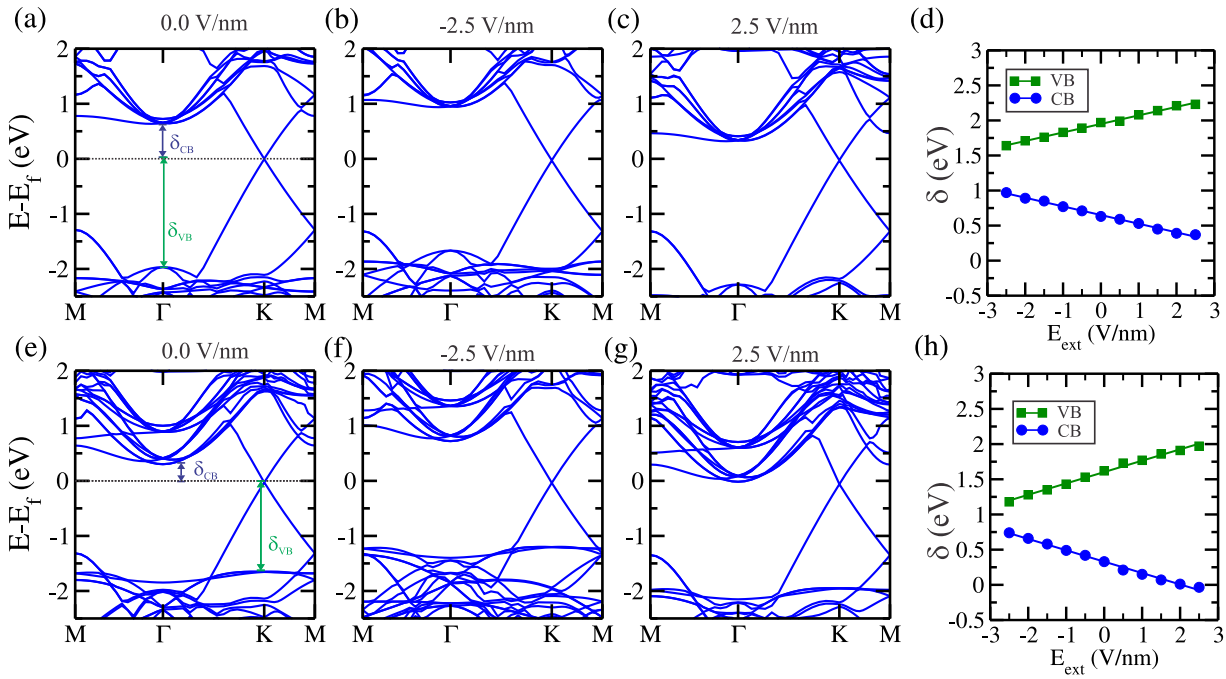

FIG. 6. (a)–(c) Evolution of the band structure as a function of the external electric field for single-layer blue phosphorus on monolayer graphene and (e)–(g) bilayer blue phosphorus. (d), (h) Evolution of the band edges as a function of the field relative to the graphene Dirac point for single-layer blue phosphorus and bilayer blue phosphorus, respectively. The electric field is applied along the $\hat{z}$ direction as defined in Fig. 1(b). The Fermi level of the heterostructures was set to zero and VB (CB) represents the top (bottom) of the valence (conduction) band. All band structures were aligned with respect to the vacuum level.

channel n type. This result is opposite to those obtained for black phosphorus on top of graphene, which predict an n-type contact [66].

The evolution of the band structures and band edges of 1 blue-P@G and 2 blue-P@G, under an applied external electric field ranging from -2.5 V/nm to $+2.5$ V/nm, in steps of 0.5 V/nm, [along the $\hat{z}$ direction; see Fig. 1(b)] is presented in Fig. 6. The transverse electric field gives rise to a potential gradient normal to the blue-P@graphene interface, making possible the tunability of the energy positions of the CB and VB of the semiconductor (blue-P) with respect to the Fermi level of the metal (G), indicated as δ_{CB} and δ_{VB} in Figs. 6(a) and 6(e). Moreover, the applied electric field lifts the degeneracy among distinct layers in few layers of blue-P. Once the degeneracy is lifted, the electronic states that are localized in regions with higher potential will have a higher energy due to electrostatic interaction with the electric field, whereas those states localized in regions with lower potential will have a lower energy. When negative external electric fields are applied [Figs. 6(b) and 6(f)], the occupied states (p_z orbitals) of the 1 blue-P (2 blue-P), initially at -2 eV, Γ point (-1.6 eV, K point) can gradually be upshifted to the Fermi energy, i.e., closer to the Dirac cone of graphene. Regarding the unoccupied states (hybridized s and $p_{x,y}$ orbitals), around the Γ point, they are upshifted (far away to the Dirac cone of graphene). If a positive electric field is applied [Figs. 6(c) and 6(g)], we verify that the unoccupied states (hybridized s and $p_{x,y}$ orbitals) of the 1 blue-P (2 blue-P), initially at $+0.5$ eV ($+0.3$ eV, K point) are linearly downshifted to closer to the Dirac cone of graphene. Under the influence of an electric field of $+2.5$ V/nm, the hybridized s and $p_{x,y}$ orbitals of the 2 blue-P become resonant to the Dirac point. Thus, an applied external electric field can insert blue-P states into the Fermi energy, generating a conduction channel. Moreover, depending on the number of blue-P layers, the electric field needed to shift these energy levels to the Fermi energy is lower.

The evolution of the band edges, δ_{CB} and δ_{VB}, as a function of the external electric field, is shown in Figs. 6(d) and 6(h). In the absence of an applied electric field, as already pointed out for both systems, the conduction band is closer to the Dirac point, leading to an n-type Schottky barrier. For negative values of the applied field, it is possible to change this Schottky barrier from n type to p type, where for the monolayer we estimate a field of -5.3 and -3.9 V/nm for the bilayer blue-P. For positive values of the electric field, for both systems, the SBH always remains n type, decreasing its value linearly with the field. Moreover, for the 2 blue-P@G heterostructure the Dirac cone is energetically below the VB of blue-P for positive values of the electric field applied higher than 2.5 V/nm, making the contact become Ohmic.

IV. CONCLUSIONS

In conclusion, based on first-principles electronic structure calculations we explore the structural and electronic properties of few layers of blue phosphorus and their vdW heterostructures with graphene. We show that the energetically most stable stack of two layers of blue phosphorus is AA_1. Besides that, for all stacking configurations, the multilayer blue phosphorus preserves its semiconducting and indirect band-gap character. Our findings also reveal that the properties of graphene and blue phosphorus are preserved upon their contact. Further, we demonstrate that it is possible to tune the position of the band structure of phosphorus relative to that of graphene through the application of an external electric field perpendicular to the system. This allows significant control of the Schottky barrier height as well as the doping of 2D blue phosphorus. The understanding of all these properties is essential for paving the path to the theoretical design of future nanodevices based on van der Waals heterostructures.

ACKNOWLEDGMENTS

This work was supported by the Brazilian agencies FAPEG, FAPEMIG, and CNPq. We would like to acknowledge computing time provided on the Blue Gene/P supercomputer supported by the Research Computing Support Group (Rice University) and Laboratório de Computação Científica Avançada (Universidade de São Paulo).

[1] Q. H. Wang, K. Kalantar-Zadeh, A. Kis, J. N. Coleman, and M. S. Strano, Nat. Nanotechnol. **7**, 699 (2012).
[2] H. Wang, L. L. Yu, Y. H. Lee, Y. M. Shi, A. Hsu, M. L. Chin, L. J. Li, M. Dubey, J. Kong, and T. Palacios, Nano Lett. **12**, 4674 (2012).
[3] J. M. Hamm and O. Hess, Science **340**, 1298 (2013).
[4] K. J. Koski and Y. Cui, ACS Nano **5**, 3739 (2013).
[5] S. Z. Butler, S. M. Hollen, L. Cao, Y. Cui, J. A. Gupta, H. R. Gutiérrez, T. F. Heinz, S. S. Hong, J. Huang, A. F. Ismach, E. Johnston-Halperin, M. Kuno, V. V. Plashnitsa, R. D. Robinson, R. S. Ruoff, S. Salahuddin, J. Shan, L. Shi, M. G. Spencer, M. Terrones, W. Windl, and J. E. Goldberger, ACS Nano **4**, 2898 (2013).
[6] P. Miró, M. Audiffred, and T. Heine, Chem. Soc. Rev. **43**, 6537 (2014).
[7] K. S. Novoselov, A. K. Geim, S. V. Morozov, D. Jiang, Y. Zhang, S. V. Dubonos, I. V. Grigorieva, and A. A. Firsov, Science **306**, 666 (2004).
[8] M. Chhowalla, D. Jena, and H. Zhang, Nat. Rev. Mater. **1**, 16052 (2016).
[9] A. J. Mannix, B. Kiraly, M. C. Hersam, and N. P. Guisinger, Nat. Rev. Chem. **1**, 0014 (2017).
[10] J. E. Padiha, R. H. Miwa, and A. Fazzio, Phys. Chem. Chem. Phys. **18**, 25491 (2016).
[11] A. J. Mannix, X.-F. Zhou, B. Kiraly, J. D. Wood, D. Alducin, B. D. Myers, X. Liu, B. L. Fisher, U. Santiago, J. R. Guest, M. J. Yacaman, A. Ponce, A. R. Oganov, M. C. Hersam, and N. P. Guisinger, Science **350**, 1513 (2015).
[12] C.-H. Hu, A. R. Oganov, Q. Zhu, G.-R. Qian, G. Frapper, A. O. Lyakhov, and H.-Y. Zhou, Phys. Rev. Lett. **110**, 165504 (2013).
[13] L.-C. Xu, A. Du, and L. Kou, Phys. Chem. Chem. Phys. **18**, 27284 (2016).
[14] S. Cahangirov, M. Topsakal, E. Aktürk, H. Sahin, and S. Ciraci, Phys. Rev. Lett. **102**, 236804 (2009).
[15] Y. Xu, B. Yan, H.-J. Zhang, J. Wang, G. Xu, P. Tang, W. Duan, and S.-C. Zhang, Phys. Rev. Lett. **111**, 136804 (2013).

[16] M. Ezawa, J. Phys. Soc. Jpn. **84**, 121003 (2015).
[17] M. Z. Hasan and C. L. Kane, Rev. Mod. Phys. **82**, 3045 (2010).
[18] L. Li, Y. Yu, G. J. Ye, Q. Ge, X. Ou, H. Wu, D. Feng, X. H. Chen, and Y. Zhang, Nat. Nanotechnol. **9**, 372 (2014).
[19] H.-S. Tsai, S.-W. Wang, C.-H. Hsiao, C.-W. Chen, H. Ouyang, Y.-L. Chueh, H.-C. Kuo, and J.-H. Liang, Chem. Mater. **28**, 425 (2016).
[20] J. Ji, X. Song, J. Liu, Z. Yan, C. Huo, S. Zhang, M. Su, L. Liao, W. Wang, Z. Ni, Y. Hao, and H. Zeng, Nat. Commun. **7**, 13352 (2016).
[21] F. Reis, G. Li, L. Dudy, M. Bauernfeind, S. Glass, W. Hanke, R. Thomale, J. Schäfer, and R. Claessen, Science **357**, 287 (2017).
[22] H. O. H. Churchill and P. Jarillo-Herrero, Nat. Nanotechnol. **9**, 330 (2014).
[23] H. Liu, A. T. Neal, Z. Zhu, Z. Luo, X. Xu, D. Tomanék, and P. D. Ye, ACS Nano **4**, 4033 (2014).
[24] A. Castellanos-Gomez, L. Vicarelli, E. Prada, J. O. Island, K. L. Narasimha-Acharya, S. I. Blanter, D. J. Groenendijk, M. Buscema, G. A. Steele, J. V. Alvarez, H. W. Zandbergen, J. J. Palacios, and H. S. J. van der Zant, 2D Mater. **1**, 025001 (2014).
[25] X. Ling, H. Wang, S. Huang, F. Xia, and M. S. Dresselhaus, Proc. Natl Acad. Sci. USA **112**, 4523 (2015).
[26] M. Akhtar, G. Anderson, R. Zhao, A. Alruqi, J. E. Mroczkowska, G. Sumanasekera, and J. B. Jasinski, npj 2D Mater. Appl. **1**, 5 (2017).
[27] H. Liu, Y. Du, Y. Deng, and P. D. Ye, Chem. Soc. Rev. **44**, 2732 (2015).
[28] M. Buscema, D. J. Groenendijk, S. I. Blanter, G. A. Steele, H. S. J. van der Zant, and A. Castellanos-Gomez, Nano Lett. **14**, 3347 (2014).
[29] M. Engel, M. Steiner, and Ph. Avouris, Nano Lett. **14**, 6416 (2014).
[30] Z. Zhu and D. Tománek, Phys. Rev. Lett. **112**, 176802 (2014).
[31] J. L. Zhang, S. Zhao, C. Han, Z. Wang, S. Zhong, S. Sun, R. Guo, X. Zhou, C. D. Gu, K. D. Yuan, Z. Li, and W. Chen, Nano Lett. **16**, 4903 (2016).
[32] J.-P. Xu, J.-Q. Zhang, H. Tian, H. Xu, W. Ho, and M. Xie, Phys. Rev. Mater. **1**, 061002(R) (2017).
[33] J. Xiao, M. Long, X. Zhang, J. Ouyang, H. Xu, and Y. Gao, Sci. Rep. **5**, 9961 (2015).
[34] A. K. Geim and I. V. Grigorieva, Nature (London) **499**, 419 (2013).
[35] G. Gao, W. Gao, E. Cannuccia, J. Taha-Tijerina, L. Balicas, A. Mathkar, T. N. Narayanan, Z. Liu, B. K. Gupta, J. Peng, Y. Yin, A. Rubio, and P. M. Ajayan, Nano Lett. **12**, 3518 (2014).
[36] D. L. Duong, S. J. Yun, and Y. H. Lee, ACS Nano **11**, 11803 (2017).
[37] T. Roy, M. Tosun, J. S. Kang, A. B. Sachid, S. B. Desai, M. Hettick, C. C. Hu, and A. J. Javey, ACS Nano **8**, 6259 (2014).
[38] Q. A. Vu, Y. S. Shin, Y. R. Kim, V. L. Nguyen, W. T. Kang, H. Kim, D. H. Luong, I. M. Lee, K. Lee, D.-S. Ko, J. Heo, S. Park, Y. H. Lee, and W. J. Yu, Nat. Commun. **7**, 12725 (2016).
[39] Y. K. Luo, J. Xu, T. Zhu, G. Wu, E. J. McCormick, W. Zhan, M. R. Neupane, and R. K. Kawakami, Nano Lett. **17**, 3877 (2017).
[40] A. Dankert and S. P. Dash, Nat. Commun. **8**, 16093 (2017).
[41] X. Qian, Y. Wang, W. Li, J. Lu, and Ju Li, 2D Mater. **2**, 032003 (2015).
[42] Y. Deng, Z. Luo, N. J. Conrad, H. Liu, Y. Gong, S. Najmaei, P. M. Ajayan, J. Lou, X. Xu, and P. D. Ye, ACS Nano **8**, 8292 (2014).
[43] B. Ghosh, S. Nahas, S. Bhowmick, and A. Agarwal, Phys. Rev. B **91**, 115433 (2015).
[44] W. Zhang and L. Zhang, RSC Adv. **7**, 34584 (2017).
[45] X. Niu, Y. Li, H. Shu, X. Yao, and J. Wang, J. Phys. Chem. C **121**, 3648 (2017).
[46] G. Kresse and J. Furthmüller, Phys. Rev. B **54**, 11169 (1996).
[47] G. Kresse and J. Furthmüller, Comput. Mater. Sci. **6**, 15 (1996).
[48] J. P. Perdew, K. Burke, and M. Ernzerhof, Phys. Rev. Lett. **77**, 3865 (1996).
[49] G. Kresse and D. Joubert, Phys. Rev. B **59**, 1758 (1999).
[50] J. Klimes, D. R. Bowler, and A. Michaelides, J. Phys.: Condens. Matter **22**, 022201 (2010).
[51] J. Klimes, D. R. Bowler, and A. Michaelides, Phys. Rev. B **83**, 195131 (2011).
[52] J. Heyd, G. E. Scuseria, and M. Ernzerhof, J. Chem. Phys. **118**, 8207 (2003).
[53] J. Heyd, G. E. Scuseria, and M. Ernzerhof, J. Chem. Phys. **124**, 219906 (2006).
[54] R. B. Pontes, R. R. Mançano, R. da Silva, L. F. Cótica, R. H. Miwa, and J. E. Padilha, Phys. Chem. Chem. Phys. **20**, 8112 (2018).
[55] J. E. Padilha, H. Peelaers, A. Janotti, and C. G. Van de Walle, Phys. Rev. B **90**, 205420 (2014).
[56] M. P. Lima, J. E. Padilha, R. B. Pontes, A. Fazzio, and A. J. R. da Silva, Solid State Commun. **250**, 70 (2017).
[57] J. E. Padilha, R. B. Pontes, and A. Fazzio, J. Phys.: Condens. Matter **24**, 075301 (2012).
[58] N. Marom, J. Bernstein, J. Garel, A. Tkatchenko, E. Joselevich, L. Kronik, and O. Hod, Phys. Rev. Lett. **105**, 046801 (2010).
[59] G. Schusteritsch, M. Uhrin, and C. J. Pickard, Nano Lett. **16**, 2975 (2016).
[60] See Supplemental Material at http://link.aps.org/supplemental/10.1103/PhysRevB.97.235419 for the bulk band gap and for the fitting of the band gap using a power law.
[61] Y. Cai, G. Zhang, and Y.-W. Zhang, Sci. Rep. **4**, 6677 (2014).
[62] R. Zhang, B. Li, and J. Yang, Nanoscale **7**, 14062 (2015).
[63] J. A. Olmos-Asar, C. R. Leão, and A. Fazzio, RSC Adv. **7**, 32383 (2017).
[64] I. Popov, G. Seifert, and D. Tománek, Phys. Rev. Lett. **108**, 156802 (2012).
[65] Y. Liu, P. Stradins, and S.-H. Wei, Sci. Adv. **10**, e1600069 (2016).
[66] J. E. Padilha, A. Fazzio, and A. J. R. da Silva, Phys. Rev. Lett. **114**, 066803 (2015).
[67] M. Sun, J.-P. Chou, J. Yu, and W. Tang, Phys. Chem. Chem. Phys. **19**, 17324 (2017).